G-SCIDAR measurements on Mt. Graham – recent results

Sebastian E. Egner[a], Elena Masciadri[b], Dan McKenna[c], T.M. Herbst[a] and W. Gaessler[a]

[a]Max-Planck-Institute for Astronomy, Koenigstuhl 17, 69117 Heidelberg, Germany;
[b]INAF - Osservatorio Astrofisico di Arcetri, L.go E.Fermi, 5. 50125 Firenze, Italy;
[c]Steward Observatory, 933 N Cherry Ave., Tucson AZ 85721-0065, U.S.A.

ABSTRACT

We present recent results of the atmospheric turbulence measured with a Generalized SCIDAR at Mt. Graham, running for 16 nights in 2004 and 2005 at the focus of the VATT Telescope. The principle of the data reduction process is shown, as well as the validation of the obtained results. From the reduced C_N^2 and wind-speed profiles, together with an estimate for the dome-seeing, the astroclimatic parameters such as seeing ϵ, isoplanatic angle ϑ_0 and wavefront coherence time τ_0 are calculated. We obtained median values for ϵ (0.67"$\pm$0.17"), ϑ_0 (2.71"$\pm$1.11") and τ_0 (3.63msec $\pm$ 1.66msec), which indicate that Mt. Graham is as an astronomical site comparable to the best ones in the world. As an application, the calculated C_N^2 profiles were used together with layer-transfer functions for a MCAO system to estimate the optimal conjugated heights of the DMs for the MCAO system of LINC-NIRVANA.

Keywords: Atmospheric Turbulence, SCIDAR, site-testing, MCAO

1. INTRODUCTION

Information about the strength and vertical distribution of the atmospheric turbulence above Mt. Graham is required for the development, construction and optimization of the sophisticated Adaptive Optics system of the LBT.[1,2] This will have a strong impact on the performance and, where still possible, on the design of the employed AO systems and control parameters. For these reasons, a dedicated site-characterization campaign with a SCIDAR instrument mounted to the VATT to measure the atmospheric turbulence above Mt. Graham is currently being performed.

1.1. SCIDAR technique

The SCIDAR (SCintillation Detection And Ranging) technique to measure the optical effects of the turbulence in the atmosphere, relies on the analysis of scintillation images generated by a binary in the pupil plane of the telescope.[3,4] The original SCIDAR method was insensitive to the turbulence near the ground, Fuchs et al.[5] thus proposed to place the detector virtually to a conjugated plane below the ground, extending the measurement range to the whole atmosphere.

From the calculated average and normalized auto-correlation of these scintillation images, the auto-correlation profile $A(r,\vartheta)$ along the axis of the binary is determined. Its logarithm $A_\chi(r,\vartheta)$ is related to the structure function of the refractive index $C_N^2(h)$ by:

$$A_\chi(r,\vartheta) \;=\; \frac{8.16\,k^2}{4\pi} \int_0^\infty C_N^2(h)\; h^{5/6}\, F(Q)\, dh, \tag{1}$$

with a Kernel function $F(Q)$. More details can be found in e.g. Klueckers et al.[6] Equation 1 is a Fredholm integral equation and can be solved by an appropriate inversion algorithm. Our system differs from the original version of the Classical[4] and Generalized SCIDAR[7] only in the numerical method used to invert the Fredholm equation. We implemented the conjugate gradient algorithm, while Avila et al.[7] uses the maximum entropy

Send correspondence to S.E. Egner, E-mail: egner@mpia.de, phone: +49 (0) 6221 528 221

Advances in Adaptive Optics II, edited by Brent L. Ellerbroek, Domenico Bonaccini Calia,
Proc. of SPIE Vol. 6272, 627257, (2006) · 0277-786X/06/$15 · doi: 10.1117/12.671418

method. In section 2.3, we will estimate which is the impact of the actual used inversion algorithm on the retrieved C_N^2-profiles.

Several Generalized SCIDAR instruments exist today and were already used for extensive observation campaigns at various astronomical observatories.[6, 8–11] We are therefore able to compare the quality of Mt. Graham as an astronomical site with other sites characterized in an equivalent way.

1.2. The Instrument

For our observations we used the SCIDAR instrument as developed by McKenna et al.[10] attached to the VATT observatory[12] with its 1.75m primary mirror. The CCD detector of the SCIDAR has 256×256 pixel (usually binned 2×2) and is coupled to an image intensifier tube. This tube is gated externally, thus achieving an effective integration time of the CCD of 1 msec, with a frame-rate of 100 Hz.

In order to adjust the conjugation height h_{GS} of the detector, the CCD attached to the image intensifier can be moved along the optical axis. We usually set h_{GS} to between 3.5 and 4.0 km below the ground. The number of frames to be averaged to get one auto- & cross-correlation image can be adjusted, we used between 3000 and 6000 frames (corresponding to 30 or 60 seconds). Also the lag in frames for the calculation of the cross-correlation images can be adjusted to between 1 and 10 frames, corresponding to a lag of 10 – 100 msec. The calculation of the correlation images are done in real-time on a dedicated DSP (Digital Signal Processor) board and only the averaged and normalized auto- & cross-correlation images are saved to disk. The same PC is also used to control the gate-generator for the image intensifier tube and the CCD camera.

2. DATA-REDUCTION

2.1. Calculation of the C_N^2 profiles

As mentioned above, we get one auto-correlation image every 30 to 60 seconds, resulting in a huge number of frames for one night of observation, making it important to have an efficient data-reduction process. In order to minimize the user interaction, we therefore designed and implemented a data-reduction pipeline in IDL. The inversion algorithm used in this pipeline to get the C_N^2-profiles is the same as the one used by Weiss[13] and Klueckers et al.[6] and will thus not be described in detail here. The algorithm used to determine the wind-speed profiles and the dome-seeing is similar to Avila et al.,[14] but still requires some user interaction in order to select the frames with well-define correlation peaks (see below). Once the C_N^2, the wind-speed profiles and the dome-seeing have been calculated, all the astro-climatic parameters (seeing ϵ, Fried-parameter r_0, isoplanatic angle ϑ_0, wavefront coherence time τ_0) are retrieved.

2.2. Determination of the Wind Profiles & Dome-Seeing

The wind speed of the turbulent layers in the first 20km above the telescope can in principle be extracted from the cross-correlation images as measured with the SCIDAR. In spite of the fact that a huge amount of data has to be analyzed, the accuracy of the results obtained with a completely automatic routine turned out to be not sufficient. We thus decided to use a semi-automatic data-reduction pipeline for the calculation of the wind-speed profiles. The user only has to select the good frames, then the determination of the intensity and the position of the peaks in the cross-correlation images is done automatically. In most of our cross-correlation images, the peaks are not "well defined", which means that the peaks are extended due to wind-shear. In such cases, a precise determination of the center position, and also the total intensity of the correlation peaks is not possible. Images with extended peaks were therefore discarded, in order to avoid inaccuracies. In the end, the wind-speed profile could be determined for only around 20% of the cross-correlation images.

From the cross-correlation images, the wind-speed profile is retrieved with a method similar to the one employed by Avila et al.[14] For the calculation of the dome-seeing, we used the intensities I_{dome} of the central peaks of the triplets belonging to the dome ($h = 0\text{km}\pm\Delta h/2$ and $v = 0\text{m/s}\pm\Delta v/2$) and sum of the intensities I_{outside} of all the triplets at an altitude of $h = 0\text{km} \pm\Delta h/2$, but with a wind-speed $v > \Delta v$. In the next step, the dome-seeing corrected C_N^2-profiles $C_N^{2*}(h)$ were determined via[14]

$$C_N^{2*}(h < \Delta h) \;=\; C_N^2(h < \Delta h) \;\cdot\; \frac{I_{\text{outside}}/\alpha(\Delta T)}{I_{\text{outside}}/\alpha(\Delta T) \;+\; I_{\text{dome}}}. \tag{2}$$

The factor $\alpha(\Delta T)$ corrects for the faster de-correlation of the turbulence outside the dome, with respect to the turbulence inside the dome. It was determined by taking cross-correlation images with different values of the temporal lag ΔT_{cc} in short sequence, assuming that the intensity of the turbulence in these two layers remains the same. For each cross-correlation image we calculated the ratio of the center peak intensities

$$R_i(\Delta T) \;=\; \frac{I_{i,\mathrm{outside}}(\Delta T)}{I_{i,\mathrm{dome}}(\Delta T)}, \tag{3}$$

$\alpha(\Delta T)$ is then determined from a linear fit to all the couples $(\Delta T,\;\; R_i(\Delta T))$. Using the slopes a and the offset b of this linear fit, $\alpha(\Delta T)$ is given by

$$\alpha(\Delta T) \;=\; 1 \;+\; \frac{a}{b} \cdot \Delta T. \tag{4}$$

Since, due to the temporal de-correlation, the slope a is negative, $\alpha(\Delta T)$ is always smaller than 1. From our data we determined

$$\alpha(\Delta T) \;=\; 1 - (0.035 \pm 0.003) \cdot \Delta T, \tag{5}$$

for ΔT in units of frames when using 100 Hz frame-rate.

2.3. Validation

In order to compare the results determined with our instrument to the ones measured at other astronomical sites, the validation of the results is extremely important. We thus used two methods to make sure that the obtained results are correct.

To validate the GS/LBT outputs, we used some auto-correlation frames measured at the focus of the 2.1m telescope with the GS/LUAN,[15] kindly provided by R. Avila. From these auto-correlation frames, we calculated the C_N^2-profiles, using both the GS/LUAN and the GS/LBT data-reduction pipelines. A comparison of two such C_N^2-profiles is shown in figure 1. As can be seen, the vertical distribution and the strength of the turbulence of the two profiles match very well. To quantify the difference between the two profiles, we calculated the relative error $\Delta\epsilon_X$

$$\Delta\epsilon_X \;=\; \frac{\epsilon_{\mathrm{LBT}} \;-\; \epsilon_{\mathrm{LUAN}}}{\epsilon_{\mathrm{LUAN}}} \tag{6}$$

of the seeing ϵ in different layers of the atmosphere. For the total atmosphere, the mean relative error $\langle\Delta\epsilon_{\mathrm{TOT}}\rangle$ considering all the sample C_N^2-profiles is 2%, for the ground-layer (below 1.5 km) $\langle\epsilon_{\mathrm{BL}}\rangle$ is 4% and for the free atmosphere (above 1.5 km) $\langle\epsilon_{\mathrm{FA}}\rangle$ is 5%. The relative errors $\Delta\epsilon_X$ for all the sample profiles are randomly distributed, with no systematic trend. Thus the GS/LBT and the GS/LUAN pipeline provide comparable results starting from the same input. Moreover, the good matching of the two C_N^2-profiles indicate that the resulting C_N^2-profile is only little affected by the numerical method used to invert the Friedholm equation.

To validate the instrument itself, we compared the seeing retrieved from the $C_N^2(h)$ profiles to the seeing measured by the guide-camera at the focus of the VATT. This camera delivers every 2 seconds the residual positions (which are used for guiding), but also the FWHM of the guide-star. A comparison between the values of the seeing measured with these two techniques is shown in figure 2. For γ Ari and λ Ori the two match very well, both follow the same temporal evolution of the seeing. However, saving the FWHM data of the guide-camera is not yet automatized and has to be done manually. For this reason, unfortunately, no data taken with the guide-camera is available for the other two stars. But the measured seeing values for the SCIDAR are continuous at the transition between the stars (e.g. at around 00:30 local time), indicating that the retrieved values for the seeing is independent of the actual star used for the SCIDAR.

For the validation of the determined wind-speed profile, we used archived meteorological data from the European Center for Medium Weather Forecast (ECMWF). They provide the wind-speed profile for discrete longitude / latitude grid-points, the closest such grid point to Mt. Graham (33°00'00"N / 110°00'00"W) was 35 km to the north. The Generalized SCIDAR permits to retrieve the wind speed only for the turbulent layers, and not for the complete atmosphere. But as can be seen in figure 3, these wind-speed at discrete heights match very well with the data from the ECMWF.

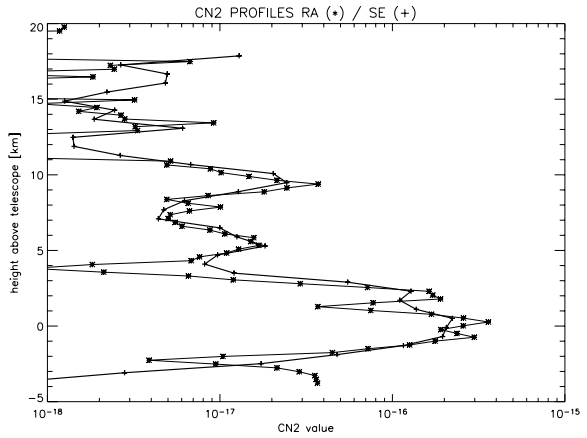

Figure 1. Comparison of the C_N^2 profiles as calculated by the GS/LUAN pipeline (⁕) and our GS/LBT pipeline (+). The vertical structure fits very well and also the determined values for r_0 differ by only 1.6%.

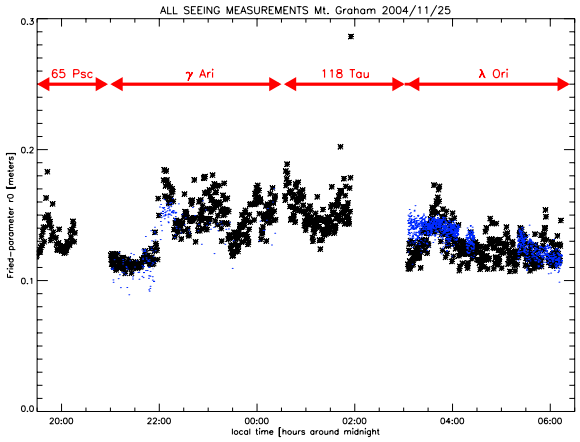

Figure 2. Comparison of the seeing values (including the dome-seeing) as determined with the SCIDAR (⁕) and the guide-camera of the VATT (blue dots). The values match very well for the two methods and follow the same temporal evolution.

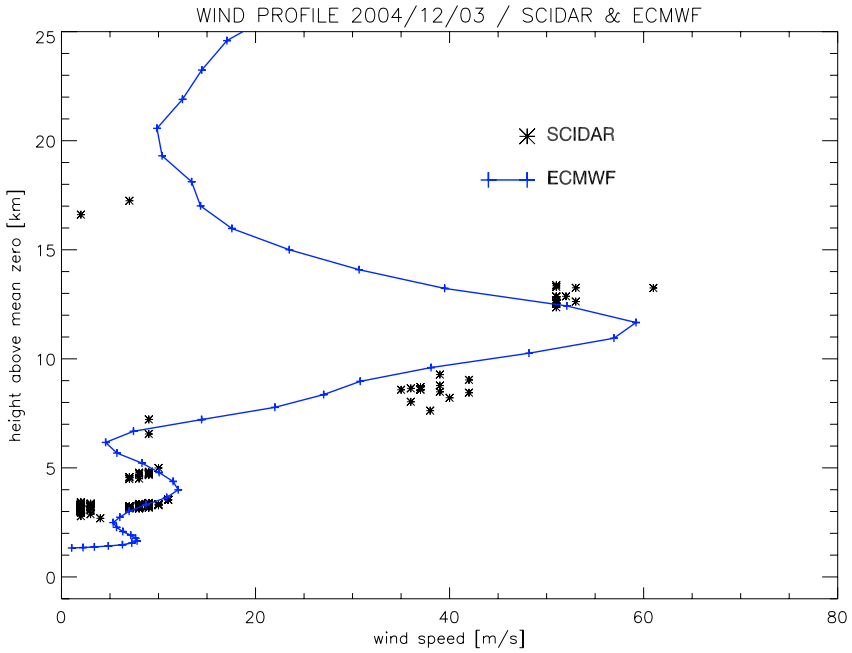

Figure 3. Comparison of the wind speed profile as measured with the SCIDAR (⁕) and as extracted from the ECMWF archive (solid line).

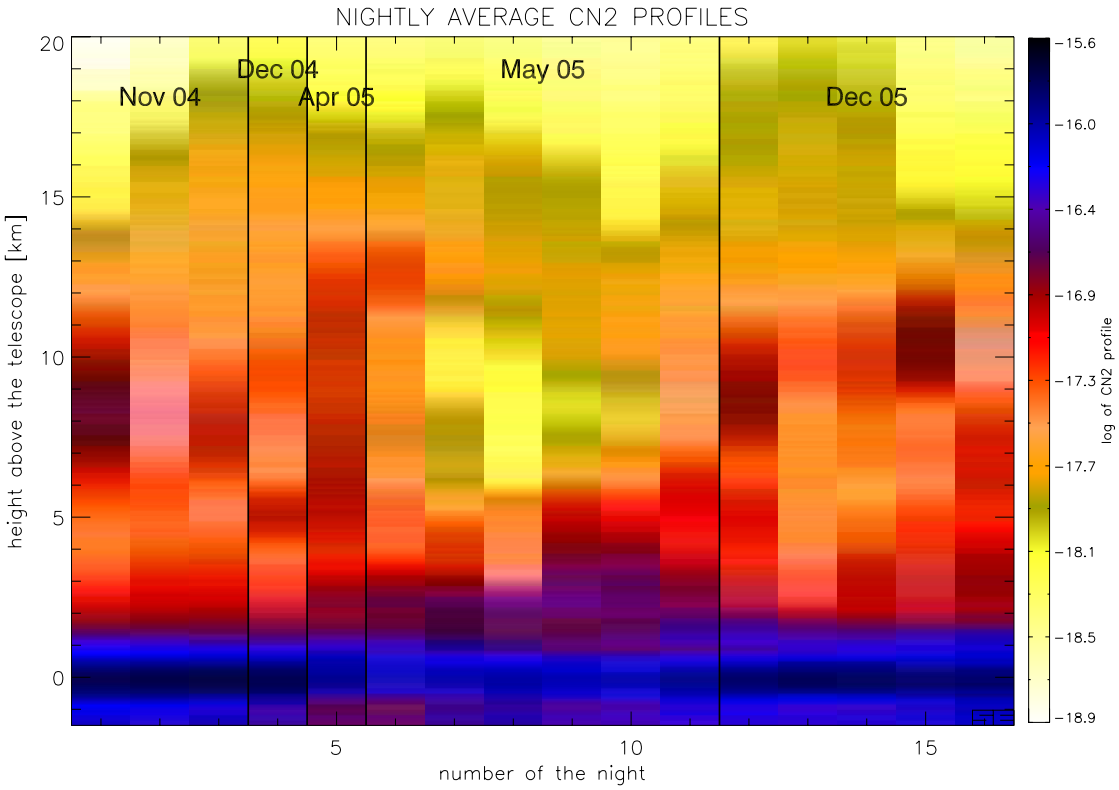

Figure 4. The mean, dome-seeing corrected, C_N^2-profiles for all the single nights. The intensity of the C_N^2 is color-coded in this plot.

3. OBSERVATIONS

In our ongoing site-characterization campaign we have measured so far around 10·000 C_N^2-profiles, distributed over 16 nights in 2004 and 2005 (see table 1). In this section, some recent results obtained with these data will be presented.

3.1. C_N^2 profiles

Figure 4 shows, for each night of observation, the mean $C_N^2(h)$ profile obtained during one night. For each C_N^2-profile, the dome-seeing has been subtracted before averaging. Figure 5 shows the median $C_N^2(h)$ profile using the data of all the 16 nights, again after correction for the contribution by the dome.

No.	Dates	No. of nights	No. of profiles
1	24 – 26 Nov. 2004	3	2707
2	03 Dec. 2004	1	383
3	26 Apr. 2005	1	554
4	19 – 24 May 2005	6	2481
5	06 – 15 Dec. 2005	5	3786
Total		**16**	**9911**

Table 1. The observing runs with the Generalized SCIDAR at the VATT for 2004 and 2005.

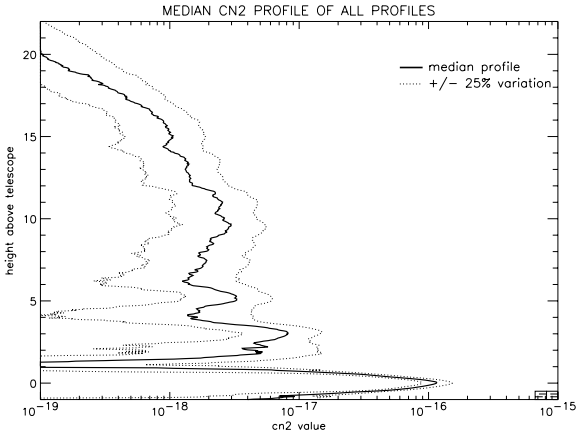

Figure 5. The median, dome-seeing corrected, C_N^2-profile for all the 16 nights.

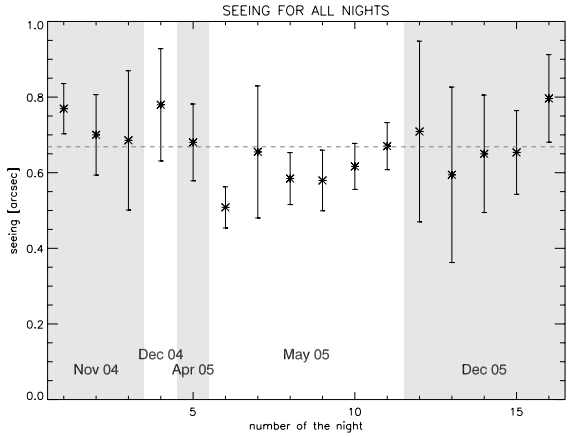

Figure 6. The median seeing values (without dome-seeing) for all the 16 nights. The error bars represent the standard deviation calculated during one night.

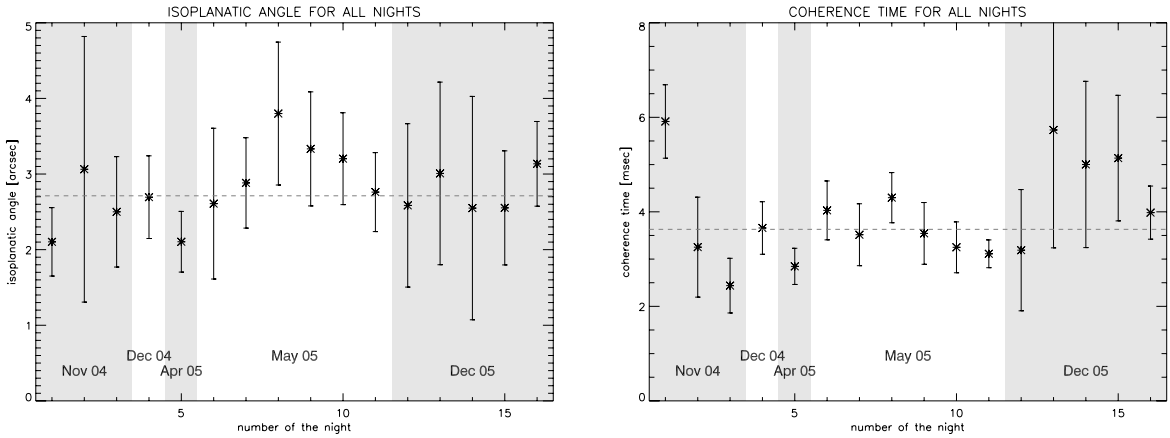

Figure 7. The values of the isoplanatic angle and the wavefront coherence time for each of the 16 nights. The error bars again represent the standard deviation calculated during one night.

3.2. Astroclimatic parameters

Using these dome-seeing corrected $C_N^2$and wind-speed profiles, the astroclimatic parameters seeing ϵ, isoplanatic angle ϑ_0 and coherence time τ_0 can be calculated. The median values obtained in each night are shown in the figures 6 and 7. Table 2 summarizes the values for ϵ, ϑ_0 and τ_0 retrieved with the Generalized SCIDAR above Mt. Graham to the ones also measured with a SCIDAR instrument at other good astronomical sites. In this table, the values for San Pedro Martir are taken from Avila et al.,[9] for Mauna Kea from Tokovinin et al.[16] and Racine et al.,[17] for La Palma from Fuensalida et al.[18] and for Cerro Tololo from Tokovinin et al.[19]

4. IMPACT FOR LINC-NIRVANA

LINC-NIRVANA is a Fizeau-interferometer, which is currently being built for the LBT. It will combine the light of the two primary mirrors interferometrically in one focus. In order to achieve a good image and achieve the spatial resolution of a 23m telescope, a good correction of the optical effects of the atmospheric turbulence is required. For this reason, LINC-NIRVANA will make use of a sophisticated Multi-Conjugate Adaptive Optics System with two deformable mirrors in each of its two arms. One is the deformable secondary of the LBT with

Site	Seeing	Isoplan. Angle	Coh. time
	arcsec	arcsec	msec
Mauna Kea	0.5 – 0.7	1.9	2.7
San Pedro Martir	0.71	1.6	6.5
Cerro Tololo	0.73	1.8	—
La Palma	0.8 – 1.5	1.3	—
Mt. Graham	**0.67±0.17**	**2.71±1.11**	**3.63±1.66**

Table 2. The median astroclimatic parameters as measured with SCIDAR instruments at various astronomical observatories as a comparison to the values as determined for Mt. Graham during our site-testing campaign.

a fixed conjugated height of 100m above the primary, the other one will be a piezo-stack DM whose conjugation height can be adjusted in real-time to between 4 and 15km. To achieve optimal performance, the conjugation height of the high-layer DM should match the vertical structure of the atmospheric turbulence. In the following, we describe how to calculate the optimal conjugation height, starting from the C_N^2-profiles measured so far, and the resulting median values.

4.1. Principle

Full end-to-end simulations of the atmosphere plus a MCAO system are rather time intensive.[20] Due to the large number of C_N^2-profiles, such simulations could thus be done only for a few, selected C_N^2-profiles. Therefore we decided to use a semi-analytic approach as proposed by Jolissaint et al.[21] With this method also the change in the optimal conjugated height of the DMs over the course of a single night can be estimated and analyzed. The idea behind this semi-analytic approach is to define so-called layer-transfer functions[22] $T(\Delta h)$. These functions describe what maximum fraction of the turbulence in a layer at distance Δh from the conjugated plane of the layer-oriented wavefront-sensor / deformable mirror can still be corrected. The total fraction of the turbulence, which can be corrected, depends of course on the parameters of the instrument (such as the number of corrected modes, loop frequency, brightness & number of guide-stars, etc.), but this fraction decreases with increasing distance from the conjugation plane due to the defocusing effect.

With the given field-of-view of the layer-oriented wavefront sensors of LINC-NIRVANA and by making some reasonable assumptions on the number of corrected modes and loop frequency these layer-transfer functions $T(\Delta h)$ can be calculated analytically. In order to keep the calculations simple and independent of the actual used guide-star configuration, we used an infinite number of guide-stars placed on a circle with a diameter of $\sqrt{1/2}$ of the maximum field-of-view. LINC-NIRVANA will use up to 12 guide-stars, resulting in $12! \approx 5 \cdot 10^8$ baselines, justifying the employed uniform filtering of the spatial frequencies, when using an infinite number of guide-stars.

From the measured C_N^2-profiles and the calculated layer-transfer functions $T(\Delta h)$, the filtered $C_N^{2*}(h)$ profiles can be calculated for given conjugation heights of the Deformable Mirrors. From the filtered $C_N^{2*}(h)$ profiles, the residual Fried-Parameter r_0 and thus the Strehl-ratio on-axis can be determined. The conjugated heights of the DMs when this Strehl-ratio is maximum, is then considered to be the optimal conjugation height $h_{i,opt}$. We used as a criteria for the optimal conjugated height the maximum Strehl-ratio on-axis. But, depending on the scientific objective of the observations, it might be of interest to have a more homogenous Strehl-ratio over the complete field-of-view. In such a case, the conjugation height of the DMs would be chosen to optimize the isoplanatic angle, resulting usually in a much higher optimal conjugation height.

4.2. Results

In figure 8 the retrieved optimal conjugated height for the high-layer DM when optimizing for Strehl-ratio on-axis over the course of one night is plotted. As can be seen, the variation in the optimal conjugation height is rather large, indicating that a real-time adjustment of the conjugation height might be required to achieve acceptable performance of the MCAO system.

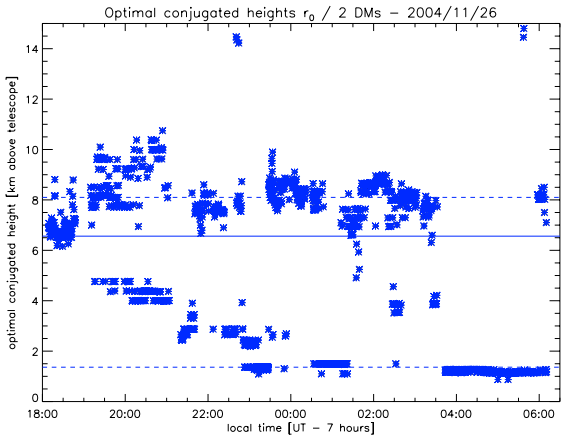

Figure 8. The temporal evolution of the optimal conjugated height for the high-layer DM for one sample night. The median value for the optimal conjugation height is for this night around 6.5km. The lines indicate the median, and the first and third quartile.

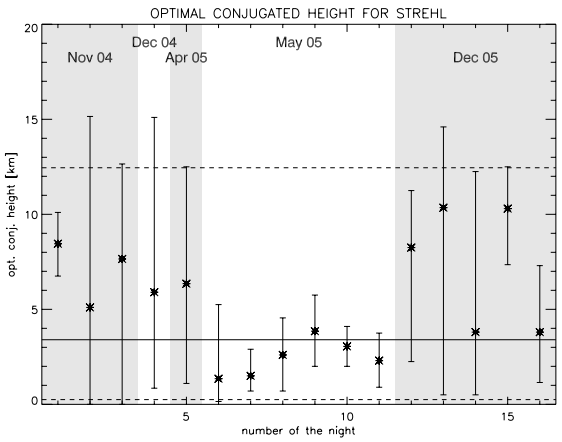

Figure 9. The optimal conjugation height for all the 16 nights when optimizing for Strehl-ratio on-axis. As the median optimal conjugation height we find 3.3km above the telescope, with quite significant differences between winter and summer.

The average optimal conjugation height $h_{\mathrm{opt,SR}}$ for optimal Strehl-ratio and $h_{\mathrm{opt},\vartheta_0}$ for optimal isoplanatic angle for all the 16 nights is shown in figure 9 and 10. The criteria used in this case to find $h_{\mathrm{opt,X}}$ is to minimize the total reduction in performance when considering all the profiles for the particular night:

$$\min\left(\sum_i R(C_{N,i}^2(h),\ h_c)\right) \qquad \Longrightarrow \qquad h_{\mathrm{opt,X}}. \tag{7}$$

The sum is over all the C_N^2-profiles for the considered night, and $R(C_{N,i}^2(h),\ h_c)$ is the relative reduction in performance when fixing the DM to the conjugation height h_c and using the C_N^2-profile number i. The resulting optimal conjugation height is slightly different from the median of the optimal conjugation height for each night (cfg. figures 8 and 9).

The same criteria was also applied to find the optimal conjugation height when considering all profiles. We

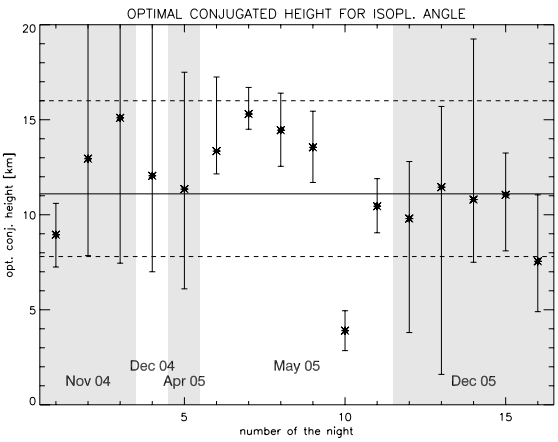

Figure 10. The optimal conjugation height for all the 16 nights when optimizing for the isoplanatic angle ϑ_0. As the median optimal conjugation height we find 11.1km above the telescope, again with a significant seasonal variation.

find an optimal conjugation height $h_{\mathrm{opt,SR}} \approx 3.3$km (for optimal Strehl-ratio) and $h_{\mathrm{opt},\vartheta_0} \approx 11.1$km (for optimal isoplanatic angle ϑ_0) above the telescope for the high-layer DM. In both cases a considerable seasonal variation is apparent. For example, during the summer, $h_{\mathrm{opt,SR}}$ is significantly lower (between 1 and 4km) than during the winter (between 6 and 11km above the telescope). However, more data is required to confirm this seasonal trend.

5. CONCLUSION

We presented a statistical analysis of Generalized SCIDAR measurements at the VATT ontop of Mt. Graham for up to now 16 nights distributed over one year and a total number of 10'000 C_N^2-profiles. The validation of the retrieved C_N^2-profiles was shown by a comparison to C_N^2-profiles reduced with a different pipeline and by comparing the calculated seeing ϵ from the C_N^2-profiles to the seeing as measured with the guide-camera of the VATT. Also the wind-speed profile as determined with the SCIDAR matches very well with the one extracted from a meteorological database.

We showed how we determined the dome-seeing and the astro-climatic parameters and found as median values for the seeing ϵ 0.67 ± 0.17 arcsec, isoplanatic angle ϑ_0 2.71 ± 1.11 arcsec and for the wavefront coherence time τ_0 3.63 ± 1.66 msec. Furthermore we studied the impact of the vertical structure of the turbulence on the MCAO system of LINC-NIRVANA. We analyzed the optimal conjugation height of the high-layer deformable mirror and found as a median value for $h_{\mathrm{opt,SR}} \approx 3.3$km and for $h_{\mathrm{opt},\vartheta_0} \approx 11.1$km above the telescope. There is a significant variation in this optimal conjugation height over single nights, but also a strong seasonal trend is apparent.

ACKNOWLEDGMENTS

The work was funded by the Alexander von Humboldt Foundation through the Wolfgang Paul Prize and is based on observations with the VATT: the Alice P. Lennon Telescope and the Thomas J. Bannan Astrophysics Facility.

Remy Avila for providing the sample auto-correlation images and C_N^2-profiles.

Sebastian Daemgen for his support during the observations at the VATT.

REFERENCES

1. S. Esposito, A. Tozzi, A. Puglisi, E. Pinna, P. Stefanini, G. Giorgetti, F. Camiciottoli, P. Salinari, P. Bianchi, and J. J. Storm, "Integration and test of the first light AO system for LBT," *5490*, p. 228, SPIE, 2004.
2. W. Gaessler, R. Ragazzoni, T. H. D. Andersen, C. Arcidiacono, H. Baumeister, U. Beckmann, J. Behrend, T. Bertram, P. Bizenberger, H. Bohnhardt, F. Briegel, E. Diolaiti, T. Driebe, A. Eckhardt, S. Egner, J. Farinato, M. Heininger, M. Kürster, W. Laun, S. Ligori, V. Naranjo, E. Nussbaum, H.-W. Rix, R.-R. Rohloff, P. Salinari, R. Soci, C. Storz, C. Straubmeier, E. Vernet-Viard, G. Weigelt, R. Weiss, and W. Xu, "LINC-NIRVANA: how to get a 23-m wavefront nearly flat," *5490*, p. 527, SPIE, 2004.
3. A. Rocca, F. Roddier, and J. Vernin, "Detection of atmospheric turbulent layers by spatiotemporal and spatioangular correlation measurements of stellar-light scintillation," *JOSA* **64**, p. 1000, 1974.
4. J. Vernin and M. Azouit, "Traitment d'image adapte au speckle atmospherique. I. Formation du speckle en atmosphere turbulente. Proprietes statistiques," *J. Optics Paris* **14**, 1983.
5. A. Fuchs, M. Tallon, and J. Vernin, "Focusing on a Turbulent Layer: Principle of the "Generalized SCIDAR"," *PASP* **110**, p. 86, 1998.
6. V. Klückers, N. Wooder, T. Nicholls, M. Adcock, I. Munro, and J. Dainty, "Profiling of atmospheric turbulence strenght and velocity using a generalised SCIDAR technique," *A&A Suppl.* **130**, p. 141, 1998.
7. R. Avila, J. Vernin, and E. Masciadri, "Whole atmospheric-turbulence profiling with generalized scidar," *Appl. Opt.* **36**, p. 7898, 1997.
8. R. Avila, J. Vernin, M. Chun, and L. Sanchez, "Turbulence and wind profiling with generalized scidar at Cerro Pachon," in *SPIE*, *4007*, p. 721, 2000.
9. R. Avila, E. Masciadri, J. Vernin, and J. Sánchez, "Generalized SCIDAR Measurements at San Pedro Mártir. I. Turbulence Profile Statistics," *PASP* **116**, p. 682, 2004.

10. D. McKenna, R. Avila, J. Hill, S. Hippler, P. Salinari, P. Stanton, and R. Weiss, "LBT facility SCIDAR: recent results," in *SPIE*, *4839*, p. 825, 2003.
11. J.-L. Prieur, G. Daigne, and R. Avila, "SCIDAR measurements at Pic du Midi," *A&A* **371**, p. 366, 2001.
12. S. West, R. Nagel, D. Harvey, B. Phillips, J. Ray, T. Trebisky, R. Cromwell, N. Woolf, C. Corbally, R. Boyle, and D. Blanco, "Progress at the Vatican Advanced Technolgy Telescope," in *SPIE*, *2871*, p. 74, 1997.
13. R. Weiß, *Point Spread Function Reconstruction for the Adaptive Optics System ALFA and its Application to Photometry*. PhD thesis, University of Heidelberg, 2003.
14. R. Avila, J. Vernin, and L. Sanchez, "Atmospheric turbulence and wind profiles monitoring with generalized scidar," *A&A* **369**, p. 364, 2001.
15. R. Avila, J. Vernin, and S. Cuevas, "Turbulence Profiles with Generalized SCIDAR at San Pedro Martir Observatory and Isoplanatism Studies," *PASP* **110**, p. 1106, 1998.
16. A. Tokovinin, J. Vernin, A. Ziad, and M. Chun, "Optical Turbulence Profiles at Mauna Kea measured by MASS and SCIDAR," *PASP* **117**, p. 395, 2005.
17. R. Racine and B. Ellerbroek, "Profiles of the nigh-time turbulence above Mauna Kea and isoplanatism extension in adaptive optics," in *SPIE*, *2534*, p. 248, 1995.
18. J. Fuensalida, B. Garcia-Lorenzo, J. Castro, S. Chueca, J. Delgado, J. Gonzalez-Rodriguez, C. Hoegemann, M. Reyes, M. Verde, and J. Vernin, "Statistics of atmospheric parameters for the Observatorio del Roque de los Muchachos," in *SPIE*, *5572*, p. 1, 2004.
19. A. Tokovinin, S. Baumont, and J. Vasquez, "Statistics of turbulence profile at Cerro Tololo," *MNRAS* **340**, p. 52, 2003.
20. C. Arcidiacono, *Multi-Conjugate Adaptive Optics for Large Telescopes*. PhD thesis, Universita degli studi di Firenze, 2004.
21. L. Jolissaint and J.-P. Veran, "Fast computation and morphologic interpretation of the Adaptive Optics Point Spread Function," in *BCAO*, p. 201, 2002.
22. M. Owner-Petersen and A. Gontcharov, "Multi-conjugate Adaptive Optics for Large Telescopes Analytical Control of the Mirror Shapes," *JOSA* **19**, p. 537, 2002.